8166–8181 *Nucleic Acids Research, 2013, Vol. 41, No. 17* *Published online 1 July 2013*
doi:10.1093/nar/gkt582

Using stable MutS dimers and tetramers to quantitatively analyze DNA mismatch recognition and sliding clamp formation

Flora S. Groothuizen[1], Alexander Fish[1], Maxim V. Petoukhov[2], Annet Reumer[1], Laura Manelyte[3], Herrie H. K. Winterwerp[1], Martin G. Marinus[4], Joyce H. G. Lebbink[5,6], Dmitri I. Svergun[2], Peter Friedhoff[3] and Titia K. Sixma[1,*]

[1]Division of Biochemistry and CancerGenomiCs.nl, Netherlands Cancer Institute, Plesmanlaan 121, 1066 CX Amsterdam, the Netherlands, [2]European Molecular Biology Laboratory, Hamburg Outstation, EMBL c/o DESY, Notkestrasse 85, 22607 Hamburg, Germany, [3]Institute for Biochemistry, Justus Liebig University, Heinrich-Buff Ring 58, D-35392, Giessen, Germany, [4]Department of Biochemistry and Molecular Pharmacology, University of Massachusetts Medical School, 364 Plantation Street, Worcester, MA 01605, USA, [5]Department of Cell Biology and Genetics, Cancer Genomics Center, Erasmus Medical Center, PO Box 2040, 3000 CA Rotterdam, the Netherlands and [6]Department of Radiation Oncology, Erasmus Medical Center, PO Box 2040, 3000 CA Rotterdam, the Netherlands

Received February 13, 2013; Revised June 7, 2013; Accepted June 11, 2013

ABSTRACT

The process of DNA mismatch repair is initiated when MutS recognizes mismatched DNA bases and starts the repair cascade. The *Escherichia coli* MutS protein exists in an equilibrium between dimers and tetramers, which has compromised biophysical analysis. To uncouple these states, we have generated stable dimers and tetramers, respectively. These proteins allowed kinetic analysis of DNA recognition and structural analysis of the full-length protein by X-ray crystallography and small angle X-ray scattering. Our structural data reveal that the tetramerization domains are flexible with respect to the body of the protein, resulting in mostly extended structures. Tetrameric MutS has a slow dissociation from DNA, which can be due to occasional bending over and binding DNA in its two binding sites. In contrast, the dimer dissociation is faster, primarily dependent on a combination of the type of mismatch and the flanking sequence. In the presence of ATP, we could distinguish two kinetic groups: DNA sequences where MutS forms sliding clamps and those where sliding clamps are not formed efficiently. Interestingly, this inability to undergo a conformational change rather than mismatch affinity is correlated with mismatch repair.

INTRODUCTION

The DNA mismatch repair (MMR) system is important to maintain genomic stability. Mismatch repair protein MutS recognizes misincorporated nucleotides, and this starts a cascade of events involving the recruitment of several proteins. This eventually results in the removal of the mismatch and resynthesis of the new DNA strand (1). Loss of MutS leads to a mutator phenotype in bacteria, and in humans mutations in MutS homologs can result in hereditary non-polyposis colon cancer, also known as Lynch syndrome (2,3). To understand the molecular impact of such mutations, the bacterial mismatch repair system is a widely used model.

In bacterial mismatch repair, MutS binds DNA in a homodimeric form. Within this dimer, there is an asymmetric association of the monomers when bound to heteroduplex DNA, as has been shown in crystal structures (4–6). After mismatch recognition, MutS exchanges adenosine diphosphate (ADP) for adenosine triphosphate (ATP) and undergoes a conformational change that allows sliding on DNA (7).

Each subunit of MutS consists of 853 amino acids in *Escherichia coli*. The currently known crystal structures of MutS bound to mismatches, however, lack a 53 amino acids long C-terminal domain. The structure of this domain has partly been elucidated fused to maltose-binding protein (MBP) (8). It has been found to be important for mismatch repair (9), although this dependence

*To whom correspondence should be addressed. Tel: +31 20 512 1959; Fax: +31 20 512 9070; Email: t.sixma@nki.nl

The authors wish it to be known that, in their opinion, the first two authors should be regarded as Joint First Authors.

could be due to decreased stability of the dimer on truncation of the C-terminal domain (8).

By interactions via these C-terminal domains, *E. coli* MutS dimers can form tetramers (K_d of 50 nM) (10), which has also been shown for other bacterial MutS homologs (11–13). Because of the unstable nature of the tetramerization, however, full-length MutS exists in equilibrium between dimers and tetramers in solution under physiological conditions in cells (~200 nM MutS monomers) (14). The biological function of the tetrameric form of MutS is still under discussion (8,15), but tetramerization is not essential for mismatch repair (8,16). It may, however, be important for other functions of MutS, such as its role in anti-recombination (16). The MutS tetramer is thus still a topic of interest (8,10,11,13,15–18).

The *E. coli* mismatch repair system is better understood and easier to reconstitute *in vitro* than eukaryotic mismatch repair. However, for the main heterodimeric human mismatch-recognition proteins (MutSα and MutSβ), tetramerization has not been reported, even though a similar double helix-loop-helix fold was observed for the C-termini of MutSβ as in the crystal structure of the dimerized C-termini of *E. coli* MutS (19).

The added variable of the dimer-tetramer equilibrium of wild-type *E. coli* MutS also complicates *in vitro* kinetic analysis of DNA binding. The DNA-binding kinetics of a single mismatch recognition unit of MutS have therefore never been studied quantitatively, instead it has only been done for the wild-type protein that still forms tetramers, where cooperative binding had to be taken into account (20). Uncoupling the dimer and the tetramer of MutS can help to make this system less complex.

Here, we achieve uncoupling of dimer and tetramer by site-specific point mutations in the C-terminal tetramerization domain and chemical cross-linking techniques, respectively. Using point mutations to prevent tetramerization rather than truncating the C-terminal domain, the stability of the dimer is not compromised (8,17). This enabled us to study both dimer and tetramer independently.

We used the stabilized full-length dimer and tetramer for structural studies to understand how the domains are organized within the proteins. Moreover, with our methods, the kinetics of DNA binding by the dimer and tetramer could be compared. This will be important for future studies to explain their relevance in DNA recognition. Elimination of the dimer-tetramer equilibrium enabled us to fit mismatch-recognition kinetics of single DNA-binding units of MutS. We used this possibility to quantitatively investigate recognition of different mismatches and to investigate sliding clamp formation by MutS.

MATERIALS AND METHODS

Wild-type and mutant MutS proteins

Full-length dimer mutants P839E or D835R were created in the *mutS* gene in vector pET-3d (4). To obtain single-cysteine MutS R848C protein, the six native cysteines in the *mutS* gene in vector pET-3d were mutated (C93A, C235S, C239A, C297S, C569S, C711V) followed by introduction of the R848C mutation. For single-cysteine His_6-MutS N162C, the N162C mutation was introduced into cysteine-free His_6-MutS in vector pET15b, which has been described previously (17,21). All mutations were introduced using the QuikChange Site-Directed or Multi Site-Directed Mutagenesis Kits (Stratagene) and appropriate primer sequences (obtained from Invitrogen), following the manufacturers protocol.

Wild-type and mutant MutS proteins were expressed and purified as described (4,6,17), except that in the final gel filtration buffer KCl was used instead of NaCl.

Cross-linking of single-cysteine MutS 848C

Reducing agent was removed from purified single-cysteine MutS R848C by loading it on a 5 ml of HiTrap desalting column (GE) that was pre-equilibrated with buffer containing no reducing agent [25 mM Hepes (pH 7.5), 300 mM KCl, 5 mM $MgCl_2$, 10% glycerol], and eluted fractions containing the protein peak were collected. ATP was subsequently added to the protein to a final concentration of 1 mM, after which 11-bis-maleimido-triethyleneglycol ($BM(PEG)_3$, Pierce) dissolved in dimethyl sulfoxide (DMSO) was added to a final concentration of 250 μM. The protein was then incubated on ice for 1 h, after which excess cross-linker was quenched by adding dithiothreitol (DTT) to a final concentration of 5 mM. The tetrameric protein was purified by size-exclusion chromatography on a Superdex 200 column in buffer A [25 mM Hepes (pH 7.5), 150 mM KCl, 5% glycerol]. Peak fractions were analyzed on SDS–PAGE, concentrated and flash-frozen until further use. See Supplementary Figure S1 for size-exclusion chromatography profile and SDS–PAGE analysis of cross-linked product.

To isolate DNA-bound complexes for small-angle X-ray scattering (SAXS) studies, cross-linked protein was incubated with excess 21-bp or 60-bp DNA (obtained from Invitrogen; 21 bp: AGCTGCCAGGCA CCAGTGTCA annealed with TGACACTGGTGCTTG GCAGCT, 60 bp: TGAAGCTTAGCTTAGGATCATC GAGGATCGAGCTCGGTGCAATTCAGCGGTACC CAATTC annealed with GAATTGGGTACCGCTGAA TTGCACCGAGCTTGATCCTCGATGATCCTAAGC TAAGCTTCA) for 25 min on ice and purified by size-exclusion chromatography on a Superdex 200 column in buffer A. Peak fractions containing the protein–DNA complexes were concentrated to multiple concentrations and flash frozen. Protein:DNA ratios in the complex were calculated using the ratio of absorption at 260 and 280 nm and absorption properties at both wavelengths of the individual components.

Size-exclusion chromatography and multi-angle laser light scattering analysis

For each protein sample, 2 mg was injected onto a Superdex 200 10/30 column in buffer [25 mM Hepes (pH 7.5), 150 mM KCl, 5 mM $MgCl_2$, 10 mM

2-mercaptoethanol]. Elution profiles were monitored at 280 nm. Protein was subjected in-line to multi-angle laser light scattering (MALLS) measurements in a Mini-Dawn light scattering detector (Wyatt Technology) on elution from the column. Data were analyzed using the Astra software (Wyatt Technology).

Crystallization, data processing and refinement

For crystallization, 100 μM MutS D835R (monomer concentration) was combined with 50 μM 21-bp DNA containing a mismatch (same 21-bp sequence as in the SAXS DNA-binding studies), and 100 μm ADP. Crystals were grown using hanging drop vapor diffusion from a well solution of 25 mM Tris (pH 8), 750 mM NaCl, 12% PEG 6000, 10 mM $MgCl_2$. Microseeding was used to improve crystal quality. Before data collection, crystals were transferred to a cryobuffer consisting of the mother liquor supplemented with 30% glycerol and flash cooled in liquid nitrogen.

Diffraction data were collected at beamline ID14-4 at the ESRF in Grenoble, France. Data reduction was performed using XDS (22) and Scala (23) in the CCP4 suite (24). The structure of the C-terminally truncated MutS:DNA complex (PDB entry 1E3M) (4) was used as a search model for structure solution using Phaser (25). Refinement jobs were carried out using REFMAC5 (26). PDB_REDO (27) was used to optimize refinement parameters for REFMAC5. During the refinement process, the structure of the dimer of the C-terminal 33 residues of MutS (8) was used as an initial model to fit the density for the C-terminal domain using the program Coot (28). Most of the structure could be modeled confidently, but electron density for the mismatch binding domain in subunit B and the C-terminal domains (823–853) is relatively weak and residues 658–669 and 749–757 of the ATPase domain of subunit A (the mismatch-contacting subunit), residues 1–25, 55–74 and 95–106 of the mismatch-binding domain of subunit B, residues 801–822 in both subunits and six bases are missing. We did not observe clear density for nucleotides in either of the two subunits of the crystallized protein, and the positions of the P-loops resembled empty nucleotide binding sites. Nevertheless, some residual difference density is present in the nucleotide-binding site of the mismatch-contacting subunit, suggesting a small fraction of ADP-bound protein in the crystal. Coordinates of the refined model of MutS D835R have been deposited in the Protein Data Bank with entry code 3ZLJ. For crystallographic statistics, see Table 1. Figures were generated using PyMOL (http://www.pymol.org).

Table 1. Crystallographic data collection and refinement statistics

Data collection	
λ (Å)	0.976
Resolution range (Å)	47.24–3.1 (3.27–3.1)
Completeness (%)	99.9 (100.0)
I/σ(I)	9.9 (2.4)
R_{merge} (%)	11.9 (61.7)
Space group	P 1 21 1
Cell dimensions	
a, *b*, *c* (Å)	110.29, 91.15, 112.86
α, β, γ (°)	90.00, 101.79, 90.00
Total no. of observations	175 019 (25 663)
Total no. of unique reflections	40 031 (5825)
Multiplicity	4.4 (4.4)
Wilson's B-factor (Å^2)	61.9
Refinement	
No. of atoms (protein + DNA)	13 234
Average B-factor (Å^2)	61.8
R_{free} reflections	2006
R_{work} (%)	22.73
R_{free} (%)	26.28
r.m.s.Z(bond)	0.365
r.m.s.Z(angle)	0.462
Ramachandran statistics[a] (preferred/allowed/outliers)	1549/18/0

Numbers within brackets refer to the highest resolution shell.
[a]Calculated using MolProbity (29).

SAXS measurements and analysis

SAXS measurements were performed at beamlines P12 and X33 (30) at EMBL Hamburg. Samples of MutS D835R were prepared in buffer containing 25 mM Hepes (pH 7.5), 250 mM KCl, 5% glycerol. MutS tetramer samples were prepared in buffer A as described earlier in the text. The samples were thawed and centrifuged at high speed for 1 min just before measurement. Samples were exposed to X-rays in a measuring cell cooled to 10°C. Data were analyzed using the ATSAS software package (31): data processing was performed using PRIMUS (32) where the Guinier plots were used to assess R_g values and data quality at low-angles (Supplementary Figure S2D), after which GNOM (33) was used to generate distance distribution plots. GNOM results were used as input for DAMMIF (34) to generate 10 independent *ab initio* models for both the dimer and the DNA-free tetramer, which were subsequently averaged using DAMAVER (35). For SAXS statistics, see Table 2. Figures were generated using PyMOL (http://www.pymol.org).

Cross-linking of single-cysteine mutant D162C

Single-cysteine His_6-MutS D162C was incubated for 10 min on ice at 10 μM concentration in buffer [20 mM Hepes (pH 7.5), 5 mM $MgCl_2$, 125 mM KCl and 1 mM ADP]. M4M cross-linker (1,4-butanediyl-bismethanethiosulfonate; Toronto Research Chemicals) or M17M cross-linker (3,6,9,12,15-pentaoxaheptadecane-1,17-diyl-bismethanethiosulfonate; Toronto Research Chemicals) was added in 5-fold molar excess over the protein and incubated for 20 min on ice. The extent of cross-linking was monitored by 6% SDS–PAGE after staining with colloidal coomassie. The gel was imaged with a video documentation system (BioRad).

Surface plasmon resonance measurements

Surface plasmon resonance (SPR) measurements were performed in a Biacore T200 system at 25°C. Unless otherwise indicated, DNA for the SPR measurements (obtained from Sigma) contained a 21-base pair long duplex (see Supplementary Table S1 for the full range of DNA sequences measured for MutS binding) with a

Table 2. SAXS data collection and statistics

	MutS D835R	Cross-linked MutS Tetramer	MutS Tetramer + 21-bp DNA	MutS Tetramer 60-bp DNA
Data-collection parameters				
Beam line	P12	X33	X33	X33
Beam geometry	$0.2 \times 0.12\,mm^2$	$2 \times 0.6\,mm^2$	$2 \times 0.6\,mm^2$	$2 \times 0.6\,mm^2$
Wavelength (nm)	0.124	0.15	0.15	0.15
s range (nm^{-1})	0.07–4.4	0.06-6.0	0.06–6.0	0.06–6.0
Exposure time (s)	1	120	120	120
Concentration range (mg/ml)	0.4–11.7	0.7–3.9	0.5–6.6	0.5–3.9
Temperature (K)	283	283	283	283
Structural parameters				
$I(0)$ (relative) [from $P(r)$]	10300 ± 200	260 ± 5	270 ± 5	490 ± 10
R_g (nm) [from $P(r)$]	4.6 ± 0.1	7.9 ± 0.1	8.2 ± 0.1	11.8 ± 0.3
$I(0)$ (relative) [from Guinier]	10400 ± 100	270 ± 10	270 ± 10	510 ± 10
R_g (nm) [from Guinier]	4.7 ± 0.1	7.8 ± 0.4	7.8 ± 0.3	11.5 ± 0.4
D_{max} (nm)	15.5 ± 0.5	27 ± 1	27 ± 1	43 ± 2
Porod volume estimate (nm^3)	307	702	707	1271
Dry volume calculated from sequence (nm^3)	217	460		
Molecular-mass determination				
$I(0)$ (relative) for BSA	4300 ± 100	60 ± 2	60 ± 2	60 ± 2
Molecular mass M_r [from $I(0)$] (kDa)	160 ± 10	340 ± 30	310 ± 30	580 ± 50
Calculated monomeric M_r from sequence (kDa)	95	95		

single-stranded DNA (ssDNA)-overhang consisting of 20 thymidines ($(dT)_{20}$). The ssDNA end was biotinylated for coupling to a Biacore streptavidin chip. The double-stranded DNA (dsDNA) end had a fluorescein moiety attached and by flowing over anti-fluorescein antibody (Invitrogen) after immobilization the DNA end was blocked. DNA was immobilized on a Biacore streptavidin chip to a maximum total signal of 7.0 RU.

For the mismatch variation experiments and the sequence context variation experiments, MutS protein was premixed with an equal volume of SPR buffer [25 mM Hepes (pH 7.5), 150 mM KCl, 5 mM $MgCl_2$, 0.05% TWEEN-20] or SPR buffer containing 2 mM ATP just before injection, and flown over the chip in SPR buffer with or without 1 mM ATP, respectively. Protein flow was maintained for 120 s, after which only SPR buffer was flown over for 240 s. Between injections of different concentrations of protein, the chip was regenerated with 0.05% SDS. Measurements were performed *in duplo*.

For the sliding clamp dissociation experiments, the DNA constructs for a GT mismatch or T insertion were immobilized, but the ends were not blocked with antibody. In all these measurements, 200 nM of MutS D835R was injected for 120 s to achieve maximum binding, after which buffer with varying ATP concentration was injected for 120 s to observe dissociation.

Initial kinetic fitting (as shown in Figure 4) was performed using the Biacore T200 Evaluation Software version 1.0. Values for K_d^{app} were determined by non-linear fitting using Graphpad Prism 4 (36) with a model for single-site binding: Response = $Max_{Response}$. [MutS]/(K_d^{app} + [MutS]), where MutS concentration was expressed as monomers. Values for K_d and k_{off} were determined using EvilFit (37,38).

For kinetic fitting for DNA binding by the tetramer, the following input for the Biacore T200 Evaluation Software was used:

$$A + B \underset{k_{d1}}{\overset{k_{a1}}{\rightleftharpoons}} AB \quad (1)$$

$$AB \underset{k_{d2}}{\overset{k_{a2}}{\rightleftharpoons}} A^*B \quad (2)$$

$$A^*B + B \underset{k_{d3}}{\overset{k_{a3}}{\rightleftharpoons}} A^*B_2 \quad (3)$$

where A = free MutS in solution; B = unbound DNA; AB = MutS bound to DNA, A^*B = MutS bound to DNA after a conformational change; A^*B_2 – MutS bound to two DNA binding sites; k_{a1}, k_{a2}, k_{a3}, k_{d1}, k_{d2}, k_{d3} are kinetic constants. A_{tot} (total amount of MutS based on concentration) and B_{tot} (maximum binding capacity of the surface) were also defined. This explicit second binding site model is applied to account for the fact that bending over does not change the mass as detected by SPR.

RESULTS

The dimer and tetramer of MutS can be stabilized separately

To study the dimer of MutS, the formation of tetramers has to be prevented. Although this can be achieved by truncating the C-terminal domains, this will also compromise the stability of the dimer (39). A previously reported crystal structure of the C-terminal domains of MutS showed a tetramerization interface formed by crystallographic symmetry (8). Mutations in this interface can

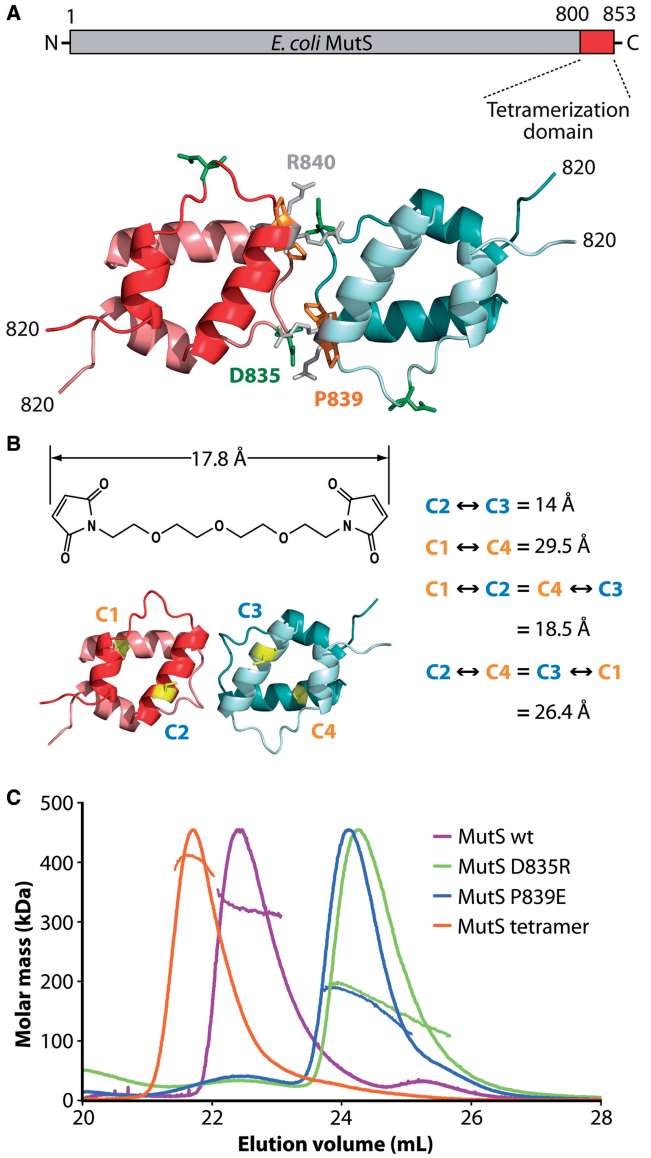

Figure 1. Stabilization of MutS dimer and tetramer. (**A**) Tetramerization of MutS can be prevented by changing the local charge in the tetramerization interface via mutation of residues in the C-terminal domains. These residues are indicated in the crystal structure of the tetramerized C-terminal domains (from PDB entry 2OK2): D835 (green), P839 (orange) and R840 (gray). (**B**) The molecular structure of the flexible molecule 1,11-bis-maleimidotriethyleneglycol ($BM(PEG)_3$) has a maximum dimension of ~18 Å. Introduced cysteines at position 848 were mapped on the crystal structure of the tetramerized C-terminal domains. The residues were mutated to cysteines in PyMOL (http://www.pymol.org) in preferred rotamer positions and are shown in yellow with the labels C1-4. Theoretical distances between sulphur atoms of these cysteines are indicated. (**C**) Normalized UV profiles and MALLS signal from size-exclusion chromatography of the full-length MutS proteins indicate apparent molecular weights of 324 kDa for wild-type MutS (purple), 410 kDa for the cross-linked tetramer (orange), 189 kDa for MutS P839E (blue) and 198 kDa for MutS D835R (green). The molecular weight of one full-length MutS monomer is 95 kDa.

perturb interactions between full-length dimers. It has been reported previously that a mutation at D835 to R, resulting in a charge inversion (Figure 1A), will prevent tetramerization of MutS without jeopardizing the stability of the dimer (17). This has also been described for an R840 to E mutation (8). We hypothesized that mutating P839 to E, introducing a negative charge (Figure 1A), will have a similar effect.

We verified the oligomerization states of the different mutants using MALLS analysis in line with size-exclusion chromatography (Figure 1C). In this measurement, wild-type full-length MutS shows a large peak for the dimer-tetramer equilibrium, with an apparent weight of 324 kDa (one monomer is 95 kDa) and a small peak corresponding to a monomer fraction. MutS D835R and P839E show molecular weights of ~198 and 189 kDa, respectively (Figure 1C), indicating that these mutants do not tetramerize. A decline in measured molecular weight toward the right ends of the peaks indicates minor dissociation into monomers, as was also observed in atomic force microscopy (AFM) studies with wild-type MutS, indicating that this is an intrinsic property of MutS (15). Nevertheless, it is much less pronounced for these full-length MutS point mutants than for the C-terminal truncation mutant ΔC800 (39). In this way, relatively stable dimers can be made via different single point mutations predicted from the published tetramer interface. We chose to use the D835R mutant for further characterization.

To stabilize the tetrameric form of MutS, chemical cross-linking was used. The residues at position 848 in the tetramerization domains are solvent-exposed and therefore appeared to be a good option for cross-linking. For this purpose, a cysteine was introduced at this position in a cysteine-free construct of full-length MutS, resulting in single-cysteine MutS R848C (SC-MutS R848C). Cysteine-free MutS is active in mismatch repair, as has been shown previously (8,17). The SC-MutS R848C mutant is fully active in mismatch repair *in vitro* (Supplementary Table S2). Its mutation rate *in vivo* is similar to wild-type with a slight elevation, owing to fluctuation in the assay or a minor defect (Supplementary Table S2). When allowing the SC-MutS R848C to chemically react with $BM(PEG)_3$, a cross-linker that contains a flexible PEG spacer and two reactive maleimides, the C-terminal domains of two adjoining dimers can be coupled together irreversibly by forming stable thioether linkages with the cysteine residues. The position of the cysteines is such that only one possible cross-link can be made with $BM(PEG)_3$ within each tetramer (Figure 1B), resulting in 50% cross-linking (Supplementary Figure S1). Size-exclusion chromatography and MALLS analysis of this purified cross-linked product indicates a molecular weight of ~410 kDa, corresponding to four MutS subunits (Figure 1C), indicating that the tetramer of MutS has been stabilized.

The C-terminal domain is mobile within the MutS dimer

The dimer-tetramer equilibrium of MutS complicates structural studies of the full-length protein. In previously reported structures of *E. coli* MutS, the C-terminal 53 residues had been truncated, which excluded the tetramerization and facilitated crystallization (4,6). The tetramerization domain has been crystallized outside the

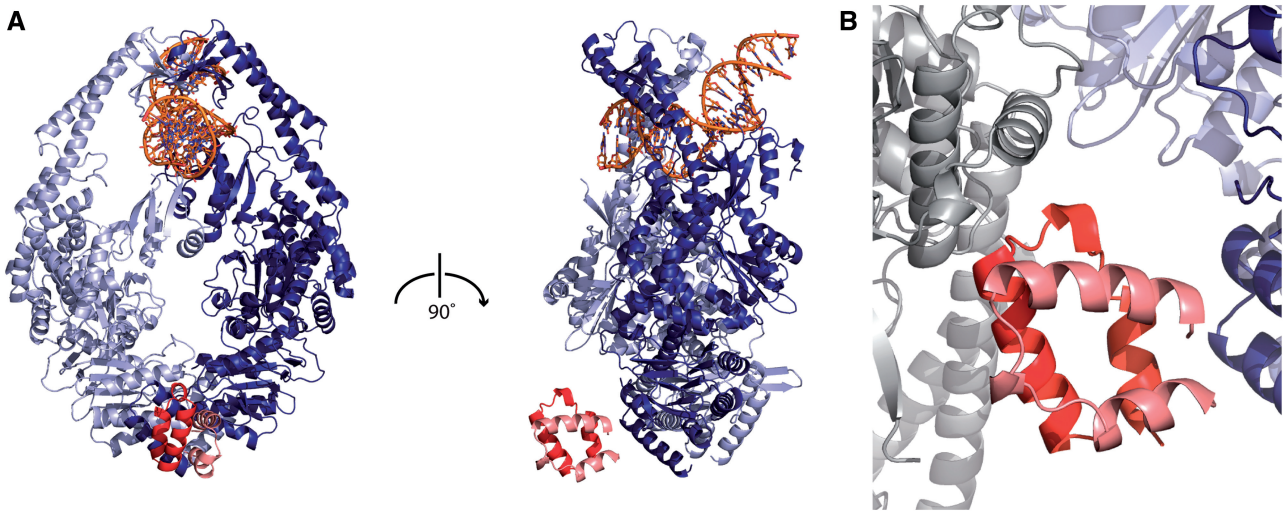

Figure 2. Crystal structure of full-length dimeric MutS D835R. (**A**) Front and side view of a cartoon representation of the dimerized C-terminal domains (red and salmon) adjacent to the ATPase domains of the rest of the dimer (dark blue and light blue). DNA is shown in orange. (**B**) The position of the dimerized C-terminal domains (red and salmon) is stabilized by crystal contacts with an adjacent MutS dimer (gray).

context of MutS, fused to MBP (8). With our current dimer mutants, the dimer-tetramer equilibrium of full-length MutS has been eliminated. We were able to crystallize full-length MutS D835R bound to a mismatch and determine the structure at a resolution of 3.1 Å (Figure 2A).

The full-length MutS protein crystallized in space group $P2_1$. The first 800 residues superpose well with previous MutS structures that were crystallized in a different crystal lattice, with an rmsd of 0.9 Å for the Cα atoms of PDB entry 1E3M. The crystal structure is almost complete except for a few missing loops (see 'Materials and Methods' section). Although we crystallized with a shorter DNA duplex [21-bp instead of 30-bp DNA (4,6,39–42)] we could resolve one more base (36 of 42 possible).

The two nucleotide-binding sites of the crystallized MutS dimer are mostly in the empty state, even though ADP was present in the crystallization mixture. This is the first *E. coli* MutS crystal structure of a nucleotide-free state, although a *Thermus aquaticus* MutS-DNA structure without nucleotide has been described (5). It has been shown by native mass spectrometry that mismatch binding regulates asymmetric nucleotide binding in *E. coli* MutS, but a nucleotide-free mismatch-bound state was also observed (43). The P-loop of subunit A is displaced compared with an ADP-bound MutS structure (4), resulting in similar empty nucleotide binding sites for subunits A and B.

This similarity between the two subunits makes the dimer more symmetrical than in ADP-bound structures, except that the N-terminal mismatch-binding domain (residues 2–115) of subunit B is in a different position than in subunit A, as it does not contact the DNA mismatch. This domain is affected by partial crystallographic disorder in subunit B and together with the connector domain it moved slightly inward compared with the existing nucleotide-bound structures, probably owing to the different crystal contacts.

Our structure includes the dimerized C-terminal domains (residues 823–853) that were truncated in previous MutS structures. Electron density for the C-terminal domains is not well defined, but we could build the two-layer helix-loop-helix fold as observed in the MBP fusion-protein structure (8), showing that this previously determined structure is present in the context of MutS. The 22 amino acids linking the C-terminal domains to the rest of the dimer could not be resolved in density, probably owing to intrinsic disorder. The chains of the two C-terminal domains can therefore not be allocated to their corresponding N-terminal subunits. It is, however, evident to which dimer in the crystal the C-terminal domains belong, as the distance to other dimers in the crystal is larger than the ~68 Å that can be spanned by 22 stretched-out residues (>75 Å to residue 800 of the nearest neighbor).

In the crystal structure, the dimerized C-terminal domains are positioned adjacent to the ATPase domains (Figure 2A). The C-termini appear to have taken the space that was occupied by residues 749–757 of subunit A as observed in other MutS structures, and these residues are not visible in our structure. Both subunits in the dimerized C-terminal domains contact helices in the connector domain of an adjacent dimer in the crystal, which probably stabilizes their position (Figure 2B).

The stable MutS D835R dimer was also used for SAXS analysis. This technique gives information on the shape of the protein and can therefore give an indication of the organization of the C-terminal domains in the full-length dimer mutant in solution. The SAXS data were used for *ab initio* modeling to obtain information about the full-length dimer shape. Lack of DNA in the measured MutS protein is expected to allow flexibility of the DNA clamp domains of MutS. This was reflected in the *ab initio*

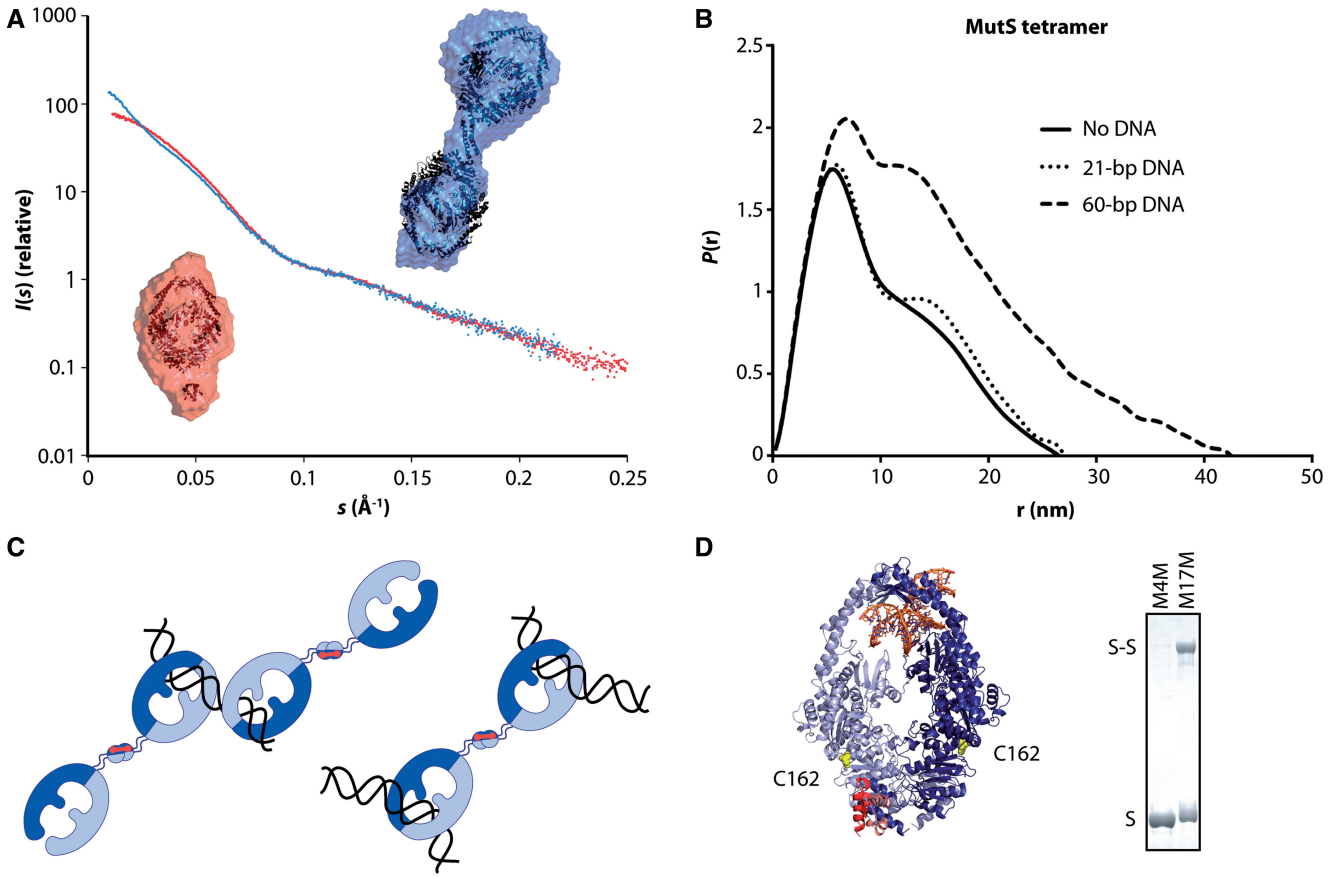

Figure 3. Conformations of the stable dimer and tetramer of MutS. (**A**) SAXS curves and *ab initio* models of the MutS D835R dimer mutant (red) and the cross-linked tetramer (blue). The scattering curves are displaced in logarithmic scale for better visualization. For the dimer envelope, the dimerized core of MutS (first 800 residues from our structure without DNA), and the dimerized C-terminal domains (residues 823–853 from our structure) are superposed onto the envelope and represented as black cartoons. For the tetramer envelope, two dimerized MutS cores and the tetramerized C-terminal domains (derived from pdb entry 2OK2) are superposed onto the envelope. (**B**) Distance distribution plot for the cross-linked tetramer of MutS: unbound (solid curve), bound to 21-bp DNA (dotted curve) and bound to 60-bp DNA (dashed curve). (**C**) Two possible models of the cross-linked tetramer of MutS bound to 60-bp DNA, which would result in a larger D_{max} values than the tetramer bound to 21-bp DNA. (**D**) Position 162 is indicated on our full-length MutS structure as yellow spheres. Using M17M cross-linker, but not M4M cross-linker, two MutS dimers can be covalently linked through cysteines at position 162 as visualized on SDS–PAGE.

models by diversion between the 10 different modeling runs. However, the overall organization of the models remained similar. Averaging of the models provided an envelope that has space for the dimerized C-terminal domains in line with the DNA-binding clamp in the dimer (Figure 3A, Supplementary Figure S2A and B), thereby extending the longest axis of the dimer.

The SAXS model is different from what was observed in the crystal structure, where the domains are positioned adjacent to the dimer. Apparently, the dimerized C-terminal domains are mobile with respect to the rest of the dimer, but in solution, there appears to be a most-occupied area extending the long axis of the dimer (Supplementary Figure S2B).

The tetramer of MutS is predominantly extended in solution but can still bend over

To get further insight into the function of the MutS tetramer, we analyzed the conformation of the tetramer in solution. Attempts to analyze tetramer conformation have been made previously for the MBP-C-terminal MutS fusion protein or for the wild-type MutS protein that is a mixture of dimeric and tetrameric states (8), but not for stable tetramers. Our cross-linked tetramer of MutS gave an opportunity to obtain more information on the shape of this oligomerization state in solution using SAXS analysis.

The SAXS data for the tetramer indicate a radius of gyration of 7.8 nm with an overall maximum dimension (D_{max}) of 26.5 nm, implying an extended conformation (Figure 3B). *Ab initio* modeling generated an envelope that can fit two MutS dimers (Figure 3A, Supplementary Figure S2C). As the C-termini of two dimers were covalently linked in our stable tetramer, this means that the DNA-binding clamps are facing away from each other in this model. These data reinforce the observation that the C-terminal domains are not adjacent to the ATPase domain but extend the long axis of the molecule.

As observed for the MutS D835R dimer, flexibility of the DNA clamp domains resulted in some diversion of the models between runs. This also biased the averaging of different models to result in an envelope in which one

dimer appears somewhat larger than the other. This can be explained by assuming that overall, the flexible unbound DNA clamp domains of the dimers in a tetramer do not occupy the same conformational volume for both dimers at the same time, resulting in an asymmetric model.

We wondered whether the tetramer would bend over and bind a single DNA molecule with both DNA-binding dimers. To investigate this, the tetramer was bound to either 21-bp DNA containing a mismatch, too short to accommodate double binding, or 60-bp DNA containing a mismatch. We then performed SAXS measurements of the DNA-bound complexes.

When incubating the tetramer with excess 21-bp DNA and purifying the resulting 1:1.8 (tetramer:DNA) complex, the SAXS measurement resulted in a curve with more distinct features than unbound tetrameric MutS (Supplementary Figure S2G). This is probably the result of reduced flexibility in the clamp domains when bound to DNA. The corresponding distance probability $P(r)$ plot reflects this with better-defined features (Figure 3B), whereas there is no significant change in the D_{max} (27 nm), indicating that the tetramer is still extended when both dimers bind a short strand of DNA.

Purification with size-exclusion chromatography after incubation with excess 60-bp DNA resulted in a 1:1.2 (tetramer:DNA) ratio, suggesting a mixture of complexes of different ratios. Although the 60-bp DNA strand would have been long enough to accommodate bending over of the tetramer to bind the DNA in two of its dimers, instead the SAXS measurement indicated that D_{max} was increased to 42.5 nm (Figure 3B, Supplementary Figure S2G). This suggests binding of multiple tetramers on DNA or two DNA strands in each tetramer in our experiment (Figure 3C). In either case, the data suggest that the tetramer remained predominantly extended when bound to DNA.

In the crystal structure of the full-length dimer, the position of the C-termini suggested the tetramer could have other conformations, using the flexible linker of the C-termini. To investigate whether occasional bending of the tetramer happens at all, a cross-linking experiment was performed for full-length His_6-MutS with a single cysteine at position 162 (Figure 3D). When incubating this protein with the reagent M4M, which can span ~8 Å, no cross-linking occurred. In contrast, when using M17M, which can span ~22 Å, a species was captured that has the connector domains linked together. This indicates that within tetramers of MutS, the two dimers can move within 22 Å of each other. We wanted to know whether the SAXS results would allow for such bending, in the light of the extended radius. In SAXS, a molecule with large intermolecular distances, such as the extended form, can dominate the scattering and there may be a mixture of conformations. We used an ensemble optimization method in which an ensemble of different random conformations is obtained, and the set that fits the scattering curve is selected (Supplementary Figures S2E and F). This analysis suggests that the SAXS data allow for co-existence of a minor population of a more bent-over form next to the major extended population. We conclude that bending over of the tetramer is possible but probably occurs relatively rarely in solution.

The MutS tetramer dissociates slower from DNA than the MutS dimer

We compared DNA-binding kinetics between the dimer and the tetramer state, using SPR analysis. To minimize effects of homoduplex binding, short DNA duplexes (21 bp) with a GT mismatch at position 11 were used. These were immobilized to a Biacore chip via a 20-base long ssDNA linker to allow for some spacing from the chip surface. The dsDNA ends had fluorescein moieties attached, which were bound by anti-fluorescein to obtain blocked ends and therefore exclude end dissociation. Dimeric MutS D835R does not bind to the ssDNA linker (Supplementary Figure S3A), and end-dissociation does not play a large role, as binding kinetics are similar for end-blocked and unblocked DNA (Supplementary Figure S3C). Using this setup, we analyzed dimer and tetramer DNA-binding kinetics separately.

The SPR measurements showed that the D835R dimer mutant dissociates completely from the DNA (Figure 4B), whereas part of the cross-linked tetramer releases relatively slowly (Figure 4C). The binding profile for wild-type MutS appears to be a combination of both dimer- and tetramer-binding kinetics (Figure 4A). A superposition of the three kinetic profiles clearly shows this difference (Supplementary Figure S3D).

The slow dissociation of the tetramer in our experiments is intriguing. When combining the cross-linked tetramer with excess 21-bp DNA for our SAXS samples, the calculated ratio for the purified complex was close to two DNA strands per tetramer. This indicates that the tetramer can be saturated with DNA in which each dimer binds a strand. This finding is in agreement with what has been found for the wild-type protein (43), although an earlier report had indicated otherwise (10). Such bivalent binding of DNA by the tetramers may explain the slow dissociation.

The slow dissociation rate of the tetramer was more pronounced when binding to 100-bp DNA or 42-bp DNA than to 21-bp DNA (Supplementary Figure S3E), but the dissociation rate did not change within the range of immobilization levels of the DNA that we used in these experiments (Supplementary Figure S3F). This suggests that in our SPR experiments, binding of the same DNA strand in the two binding sites via bending over of the tetramer or flexibility of the DNA (44) may play a role here, while at our immobilization levels 'bridging' between two immobilized DNA strands does not happen. When we use DNA that is too short for bending over (21 bp without ssDNA linker), the tetramer fully dissociates (Supplementary Figure S3G), showing that aggregation on the chip does not occur under our experimental conditions. Therefore, we conclude that the slow dissociation is due to bivalent binding of the same DNA strand by the MutS tetramer.

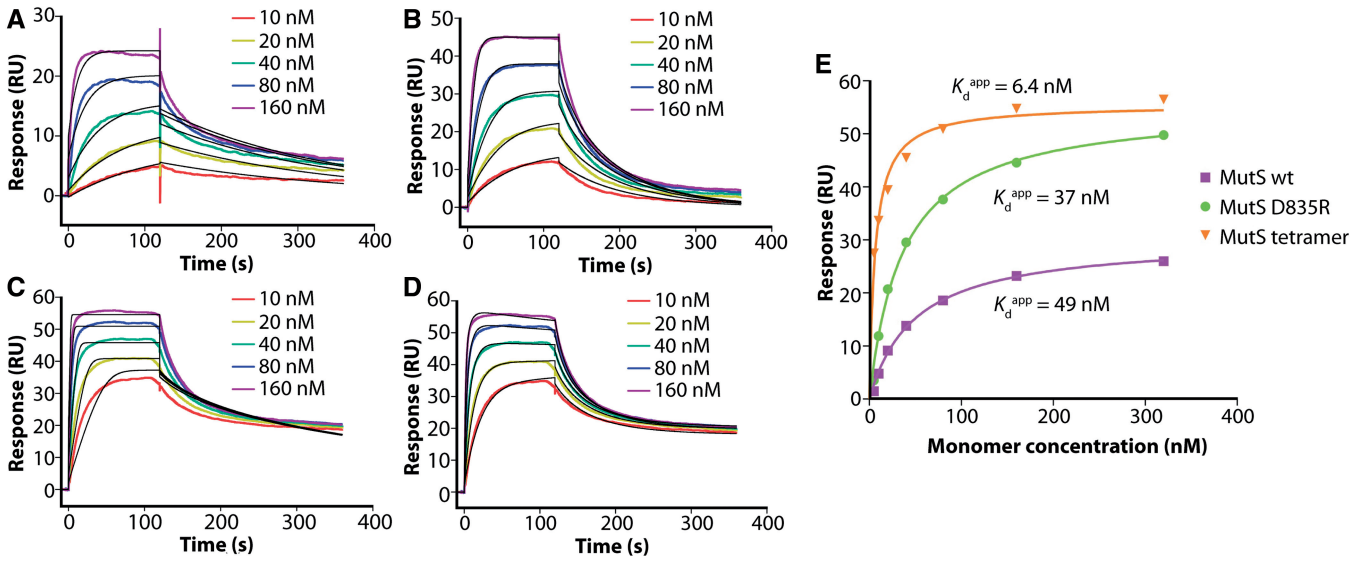

Figure 4. DNA binding by the MutS dimer and tetramer. SPR measurements of binding (**A**) wild-type MutS, (**B**) dimeric MutS D835R or (**C**) the cross-linked tetramer of MutS to a G·T mismatch. Different protein concentrations are represented by different colors (legend refers to monomer concentrations) and black lines indicate fitted kinetics using a one-phase binding model (fitted with Biacore T200 Evaluation Software). (**D**) The kinetics of the tetramer of MutS fitted using a model that takes into account bivalent binding and a conformational change, represented in black lines (fitted with Biacore T200 Evaluation Software as specified in the 'Materials and Methods' section). (**E**) Determination of K_d^{app} for the dimer and tetramer using SPR signal at equilibrium for different protein concentrations binding to the DNA [fitted with Graphpad Prism (37)].

Kinetic analysis of MutS binding to DNA is possible when dimer and tetramer are uncoupled

Wild-type MutS can bind DNA as dimers or as tetramers. Reports differ on whether binding to heteroduplex DNA shifts the dimer-tetramer equilibrium to either side (10,17,43,45), but we observed both the DNA-bound dimer and the DNA-bound tetramer at MutS concentrations up to 300 nM in an electrophoretic mobility shift assay (Supplementary Figure S3B). As the contribution of the dimer and tetramer to DNA binding can be different for every protein concentration, kinetic fitting of SPR assays is made increasingly complex, as illustrated by bad overlap of the model with the SPR data when using a one-phase binding model for fitting (Figure 4A).

Elimination of the tetramer from the equilibrium resolves the complications of wild-type protein, as a single DNA-binding unit is a dimer of MutS. Therefore, DNA binding by dimeric MutS D835R can be fitted using one-phase binding kinetics as shown by good overlap of the fitted model with the data curves (Figure 4B).

Such a simple binding mode is clearly not the case for the tetramer of MutS (Figure 4C). However, tetramer kinetics can be fitted with a model that takes into account the presence of two DNA-binding sites and a conformational change that needs to occur to bring the second site toward the same strand of DNA as described in the 'Materials and Methods' section (Figure 4D).

The tetramer displays stronger overall affinity for DNA than wild-type and dimeric MutS, as seen from the apparent dissociation constants (K_d^{app}) determined using the response at equilibrium binding for different protein concentrations as specified in the 'Materials and Methods' section (Figure 4E). This is in-line with the bivalent binding by the tetramer. The K_d^{app} values for wild-type and dimeric MutS, however, are comparable. Such similarity between the binding affinities for wild-type and dimeric MutS is in agreement with a previous report (17). The dissociation from DNA for wild-type MutS is slower than for the dimer (Figure 4A and B), probably owing to partial tetramerization, which enables bivalent DNA binding. At the same time, the time needed for tetramerization also slows down the association of wild-type MutS on DNA, explaining the similar overall affinities.

MutS binds different mismatches with different affinities, greatly influenced by flanking sequences

To investigate differences in kinetics, we measured binding of dimeric MutS D835R to all possible single mismatched bases and up to four G or C insertion loops (Table 3, Figure 6A, Supplementary Figure S4). Mismatches at position 11 in the 21-bp dsDNA were varied while the flanking sequences remained constant (see Supplementary Table S1). As controls, measurements of binding to non-mismatched sequences were included.

In our assays, the DNA on the Biacore chip is not static, but may differ slightly in orientation over the whole chip surface. Therefore, when the kinetic parameters are defined without assuming homogeneous binding, more accurate kinetic fitting of mismatch binding by the MutS dimer can be achieved. This can be done using the program EvilFit (37,38), which determines the presence of populations with similar values for dissociation rates (k_{off}) and dissociation constants (K_d) (Figure 5A and C). From the heat map, it can be derived that binding of

Table 3. Quantitative measurements of binding of dimeric MutS D835R to end-blocked 21-bp DNA of different sequences, as determined with SPR

Ligand DNA	K_d^{app} - no ATP		K_d^{app} - 1 mM ATP		k_{off} - no ATP		k_{off} - 1 mM ATP	
	in μM	(SD)	in μM	(SD)	in s^{-1}	(SD)	in s^{-1}	(SD)
Mismatch								
AT*	1.44	(0.18)	2.52	(0.76)	>0.4		>0.4	
TA*	2.17	(0.15)	1.90	(0.16)	>0.4		>0.4	
GC*	1.85	(0.71)	1.80	(0.13)	>0.4		>0.4	
CG*	1.90	(0.59)	1.58	(0.40)	>0.4		>0.4	
GA	2.01	(1.2)	1.17	(0.47)	>0.4		0.0153	(0.0014)
AG	1.60	(0.067)	0.35	(0.12)	>0.4		0.0215	(0.0018)
CA	0.115	(0.040)	0.061	(0.017)	0.0353	(0.0057)	0.0162	(0.0021)
AC	1.31	(0.39)	0.344	(0.087)	>0.4		0.0188	(0.0038)
GT	0.0809	(0.0047)	0.131	(0.021)	0.0233	(0.0033)	0.0173	(0.0024)
TG	0.231	(0.084)	0.0837	(0.051)	0.119	(0.038)	0.0175	(0.0020)
CT	0.622	(0.15)	0.443	(0.053)	>0.4		0.0186	(0.0028)
TC	1.47	(0.39)	0.634	(0.10)	>0.4		0.0191	(0.0011)
TT	2.32	(1.1)	1.38	(0.47)	>0.4		0.0162	(0.0046)
AA	0.377	(0.18)	0.0511	(0.019)	0.180	(0.11)	0.0171	(0.0024)
CC	1.50	(0.15)	1.52	(0.23)	>0.4		>0.4	
GG	0.119	(0.026)	0.0742	(0.015)	0.0298	(0.020)	0.0165	(0.0018)
Tx	0.0249	(0.0037)	0.0345	(0.011)	0.00620	(0.0010)	0.0119	(0.0017)
xT	0.155	(0.069)	0.0445	(0.014)	0.0564	(0.014)	0.0198	(0.0062)
Ax	0.187	(0.11)	0.0753	(0.046)	0.116	(0.055)	0.0168	(0.0021)
xA	0.143	(0.070)	0.0423	(0.0033)	0.0626	(0.018)	0.0178	(0.0035)
Cx	0.542	(0.10)	0.128	(0.090)	0.346	(0.011)	0.0169	(0.000071)
xC	0.192	(0.079)	0.112	(0.044)	0.0999	(0.043)	0.0162	(0.0014)
Gx	0.0382	(0.0010)	0.0375	(0.012)	0.0186	(0.0038)	0.0138	(0.0016)
xG	0.309	(0.17)	0.0523	(0.019)	0.241	(0.032)	0.0182	(0.0035)
C2	0.136	(0.012)	0.0695	(0.013)	0.122	(0.073)	0.0174	(0.0033)
C3	0.288	(0.11)	0.102	(0.041)	>0.4		0.0243	(0.0089)
C4	1.07	(0.29)	0.450	(0.069)	>0.4		0.0254	(0.0024)
G2	0.0514	(0.010)	0.0358	(0.0030)	0.0297	(0.0045)	0.0188	(0.00057)
G3	0.130	(0.068)	0.0332	(0.0032)	0.118	(0.034)	0.0178	(0.0028)
G4	0.578	(0.12)	0.135	(0.028)	0.244	(0.11)	0.0205	(0.0074)
Sequence context								
GT-1	0.0809	(0.0047)	0.131	(0.021)	0.0233	(0.0033)	0.0173	(0.0024)
GT-2	0.231	(0.084)	0.0837	(0.051)	0.119	(0.038)	0.0175	(0.0020)
GT-3	0.278	(0.13)	0.0616	0.014)	0.0999	(0.0030)	0.0134	(0.0029)
GT-4	0.0962	(0.042)	0.0380	(0.011)	0.0440	(0.0095)	0.0168	(0.0021)
GT-5	0.0480	(0.012)	0.0387	(0.0047)	0.0219	(0.0018)	0.0111	(0.00064)
GT-6	0.0550	(0.0023)	0.0327	(0.0061)	0.0118	(0.0047)	0.0100	(0.0015)
GT-7	0.0400	(0.0035)	0.0464	(0.0072)	0.0183	(0.022)	0.0105	(0.0011)

K_d^{app} and k_{off} values in the absence of ATP or in the presence of 1 mM ATP were determined as described in the 'Materials and Methods' section and expressed in monomers of MutS. Values represent averages of two measurements and standard deviations are shown within brackets. The asterisk indicates normal (Watson–Crick) base pairing in the same sequence context, an 'x' indicates a single insertion of the indicated base, and the numbers 2–4 indicate two to four base insertions in the sequence. Binding to a GT mismatch was measured in the context of different flanking sequences. See Supplementary Table S1 for full duplex sequences.

dimeric MutS D835R to a GT mismatch can be represented as a sum of single binding events within one population, whereas minor background noise can be observed as gray areas.

The possibility of kinetic analysis for dimeric MutS binding to DNA using SPR enabled us to quantitatively investigate DNA binding by a single mismatch-recognition unit of MutS for different mismatches. Values for k_{off} higher than 0.4 per second, however, were too fast to be determined. Consequently, as kinetic K_d determination using fitting dependent on simultaneous estimation of k_{off} values, the K_d could not be determined with this method for fast release of MutS. Therefore, we estimated apparent affinities K_d^{app} using the equilibrium binding (see 'Materials and Methods' section), which could be calculated for every mismatch. The K_d^{app} determined with this method correlates well with those K_d values that could be determined using kinetic fitting with EvilFit (Figure 5B and D). In this way, we compared kinetics for binding to all the different DNA mismatches.

The experiment showed that for different mismatches, the K_d^{app} and k_{off} values vary greatly: values of 25 nM – 2.3 μM are observed for K_d^{app} and values of 0.0062 to higher than 0.4 s^{-1} are observed for the dissociation rates. As expected, the homoduplexes had weaker K_d^{app} values than most of the mismatched sequences. The strongest affinity determined in absence of ATP was for binding a single thymidine insertion, and MutS had only weak affinity for TT, AG or CC mismatches, which were in the K_d^{app} range of homoduplex binding. These mismatches

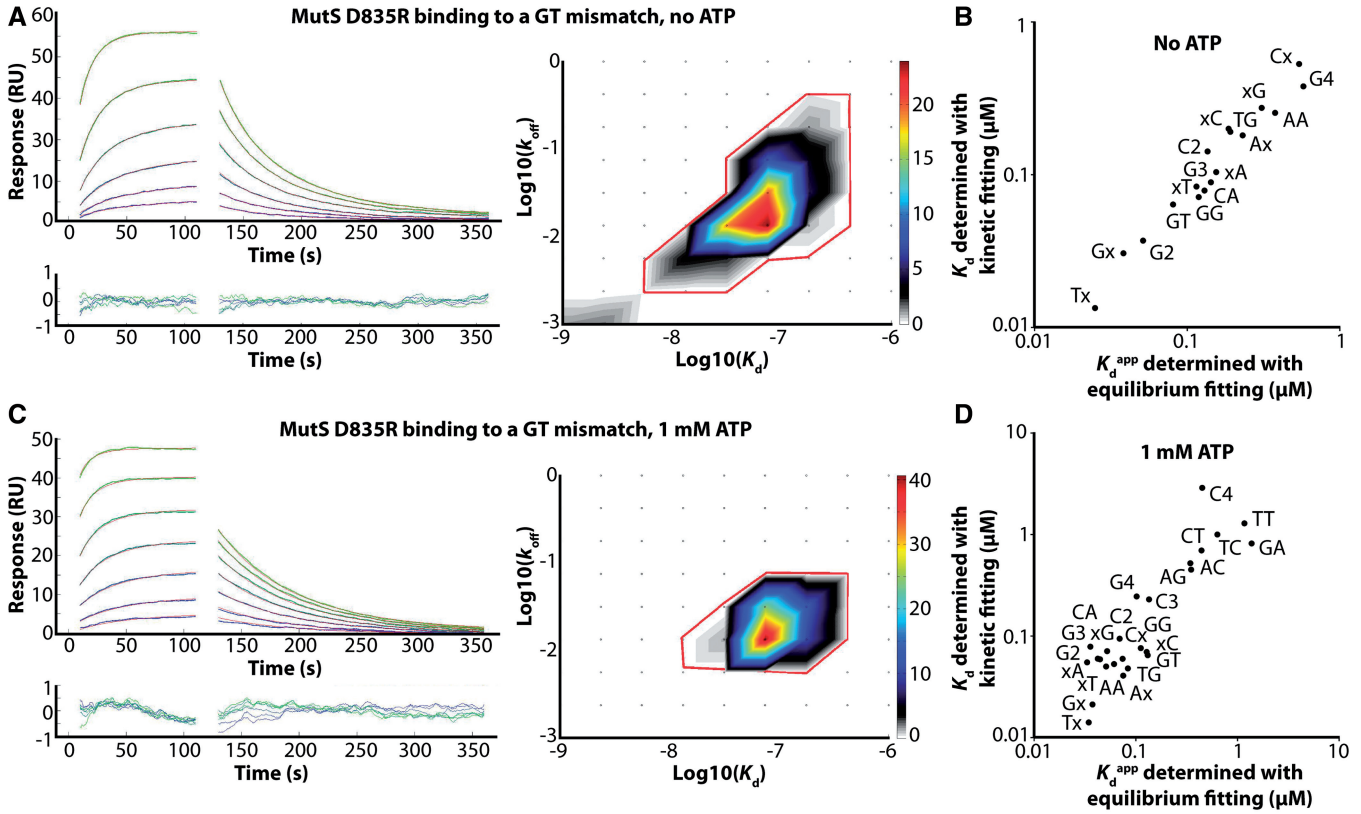

Figure 5. Kinetic fitting of the mismatch binding with EvilFit software (38,39). (**A**) Example of fitted DNA-binding kinetics of dimeric MutS D835R in absence of ATP. In the left graph, data are represented in a gradient of green to blue colors for multiple protein concentrations, and red lines indicate fitted model curves. Injection peaks were removed from the data point; thus, they would not be fitted. Residuals of the fits are plotted below the graph. Right panel shows a heat map of the *k*off and K_d distribution. A red line is drawn around the area for which a weighted averaged was taken for determination of the kinetic parameters. (**B**) Correlation between the K_d values for different mismatches that could be determined with EvilFit, and the K_d^{app} values that were determined using equilibrium binding [fitted with Graphpad Prism (37) as specified in the 'Materials and Methods' section]. Values shown are averages of two binding experiments in absence of ATP. Data points are labeled with mismatches for which binding was measured. (**C**) Example of fitted DNA binding kinetics of dimeric MutS D835R in presence of 1 mM ATP. (**D**) Correlation between the K_d values for different mismatches that could be determined with EvilFit, and the K_d^{app} values that were determined using equilibrium binding. Values shown are averages of two binding experiments in presence of 1 mM ATP.

have been shown to have low affinities in other experiments as well (39,46,47). Stronger affinities correlated with slower dissociation rates (Figure 6A, left graph), indicating that MutS binds tighter and longer to certain DNA mismatches than to others, which is in agreement with previous results on MutS and MutSα (20,48).

For all mismatches, both possible directions were analyzed: for example, binding to both GT and TG were measured. Even within such pairs of mismatches, differences were observed for K_d^{app} (81 nM for GT; 231 nM for TG) and for k_{off} (0.023 s^{-1} for GT; 0.12 s^{-1} for TG). It appears that the context of the mismatch within the DNA duplex has an effect on binding by MutS, as our tested duplexes were not palindromic around the mismatches and MutS binds to GT mismatches in a preferred orientation (49). To verify that sequence context influences mismatch binding, a range of sequences was tested in which the mismatch was kept constant and the positions of the flanking sequences were varied. Indeed, for all seven duplex sequences tested, K_d^{app} and k_{off} values differed (Table 3 and Figure 6B).

Moreover, we observed a difference in the binding preference for the mismatches when changing their direction in the DNA sequence. The order of affinities of the MutS dimer for single-base mismatches is as follows: Tx > Gx > GT > CA ~ GG > Ax > AA > Cx > CT ≫ CC - GA > TT (where an x indicates an insertion of the indicated base), whereas in opposite direction of these mismatches in the same DNA duplex, the order of affinities is as follows: GG > xA ~ xT > xC > TG > xG > AA ≫ AC > TC ~ CC > AG > TT. This means that sequence context is of greater influence on some mismatches than on others, explaining differences between the orders of affinities found in different experiments (20,46,50). The change in affinity when changing direction of the mispair in the DNA sequence is pronounced for a single G insertion or for a CA mismatch: 8-fold and 11-fold, respectively. Such a large difference for CA compared with AC was not observed in a previous report (47), indicating that the effect is dependent on the flanking sequences that are used.

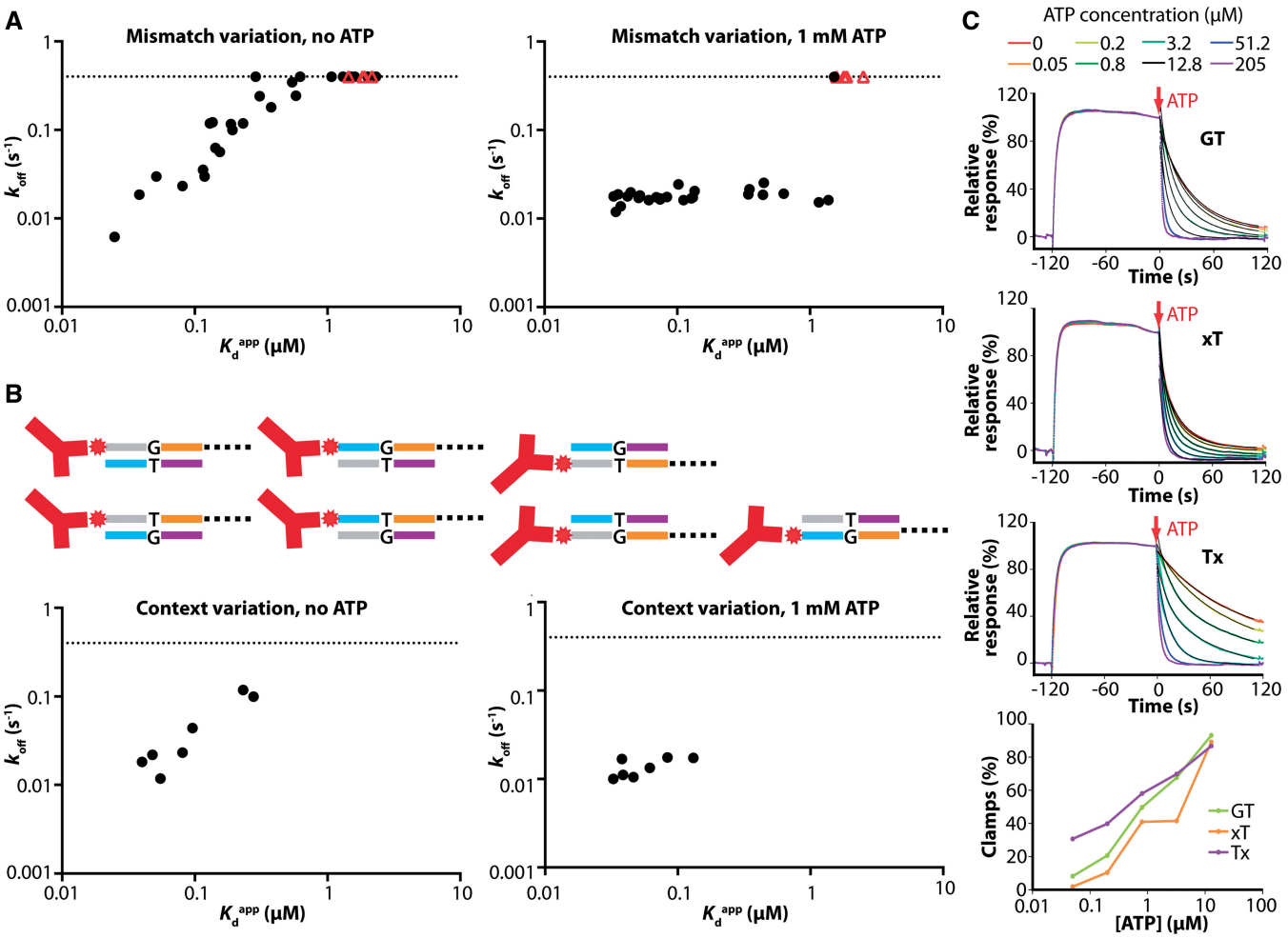

Figure 6. Mismatch binding and sliding clamp formation by dimeric MutS. (**A**) Quantitative measurements of binding of dimeric MutS D835R to 21-bp DNA of different sequences (see Supplementary Table S1) as determined with SPR. Measured values for k_{off} [determined with Evilfit (38,39)] are plotted against K_d^{app} [determined with Graphpad Prism (37) as specified in the 'Materials and Methods' section] in the absence (left graph) and the presence (right graph) of ATP for different mismatches. Values for k_{off} larger than $0.4\,s^{-1}$ could not be determined and were plotted on the dotted line at $0.4\,s^{-1}$. Red triangles indicate measurements for binding homoduplex sequences. (**B**) Variation of flanking DNA sequences around a GT mismatch is schematically represented by colors. To achieve blocked DNA ends, anti-fluorescein antibodies were bound to fluorescein moieties (both represented in red) that were coupled to the DNA strands. ssDNA linkers attaching the DNA duplex to the surface of the chip are indicated by dashed lines. Measured values for k_{off} are plotted against K_d^{app} in the absence (left graph) and the presence (right graph) of ATP for binding to a GT mismatch in the context of different flanking sequences. (**C**) MutS sliding clamp formation was investigated for three mismatches by binding dimeric MutS D835R to unblocked DNA, and subsequently releasing the MutS with buffer with increasing ATP concentrations at the time point indicated by the red arrow (top three graphs). Using fixed kinetics for the slow release observed in absence of ATP, the contribution of a faster release corresponding to the percentage of sliding clamps formed could be estimated for each ATP concentration (bottom graph).

In presence of ATP, MutS efficiently forms sliding clamps except when binding homoduplex or a CC mismatch

We investigated the effect of mismatch variation on DNA binding in the presence of ATP. This is representative for the *in vivo* situation, where ATP is present, and MutS would then be able to undergo a conformational change to form sliding clamps on DNA, the next step in MMR (7,39,51). Similar to the mismatch-binding experiments without nucleotide, we used end-blocked DNA so that sliding clamps could not slide off the DNA ends, which would make their off-rates too fast to determine. In the presence of ATP, the dissociation rates of MutS D835R were lower than without nucleotide and similar (between $0.012\,s^{-1}$ and $0.025\,s^{-1}$) for almost all mismatches, whereas for homoduplex sequences, MutS still showed a fast dissociation rate ($>0.4\,s^{-1}$) (Figure 6A, right graph; Table 3). This indicates that our assay is mismatch specific, where the fast dissociation rate indicates direct dissociation and the slow dissociation rates indicate sliding clamp formation and then dissociation, thus reflecting the stable nature of the sliding clamps (7,51). In our experiment, these slow dissociation rates of sliding clamps would dominate over any faster release by direct dissociation. Strikingly however, although we observed that most mismatches induce formation of the stable MutS sliding clamp, the CC mismatch released MutS with a dissociation rate similar to a homoduplex. This indicates that a sliding clamp is hardly formed when MutS binds this mismatch.

Affinities of MutS for the different mismatches that all form a sliding clamp still varied over 40-fold in the presence of ATP (ranging 33 nM–1.4 μM, Table 3). This indicates that the efficiency of the binding and changes toward the clamp state still differs, even though the sliding clamps formed are all equally stable. The effect of ATP on K_d^{app} values is also greater for some mismatches than for others, resulting in a different order of affinities than in absence of ATP. Still, T or G insertions can be good substrates, and TT and GA mismatches are bad substrates with affinities in the same range as homoduplex binding.

To investigate the efficiency of sliding clamp formation after binding mismatches, we performed an SPR experiment in which MutS was bound to mismatch-DNA without blocked ends in absence of ATP and was subsequently released by flowing over buffer containing different concentrations of ATP (Figure 6C). In the case of low concentrations of ATP, two components play a role: a slow dissociation rate for ATP-independent release (as in Figure 7A, yellow arrow), and a faster dissociation owing to sliding clamps releasing from the free DNA ends (Figure 7A, green arrow). The fast dissociation was more pronounced with increasing ATP concentrations as can be seen in the graphs. Using fixed kinetic parameters for the slow ATP-independent release, the contribution of the fast dissociation could be estimated for each ATP concentration, which would be representative of the efficiency of sliding clamp formation (Figure 6C, bottom graph). This revealed that for the mismatches tested, efficiency of MutS sliding clamp formation varied at low ATP concentrations. Kinetics at 51.2 μM and 205 μM ATP were too fast to be fitted, but already at ATP concentrations higher than 12.8 μM, >86% of the MutS dimers are released as sliding clamps from the three mismatches tested. Thus, except for CC, at physiological ATP concentrations, the dissociation from DNA is dominated by sliding clamp formation rather than the mismatch and its environment.

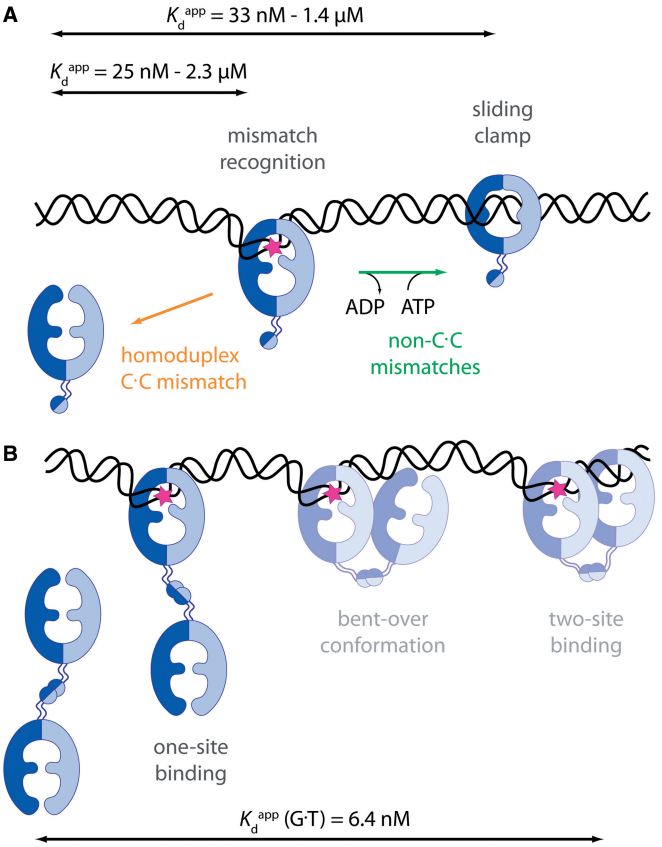

Figure 7. States of MutS. (**A**) MutS recognizes a mismatch (pink star) as a dimer. Except when binding homoduplex or a CC mismatch, MutS then exchanges its ADP for ATP and undergoes a conformational change to form a sliding clamp on DNA. Apparent dissociation constants as determined with SPR are indicated. (**B**) MutS tetramers can bind DNA in each of the two dimers by occasionally bending over. The apparent dissociation constant as determined with SPR of the MutS tetramer for DNA with a GT mismatch is indicated.

DISCUSSION

In this research, mutagenesis and chemical tools were used to stabilize the dimeric and tetrameric states of *E. coli* MutS. The full-length MutS mutants D835R and P839E abolished tetramerization but formed more stable dimers than the C-terminally truncated MutS (8) and are thus more representative for DNA mismatch repair. The stabilization of the dimer and tetramer greatly reduced the complexity caused by a dimer-tetramer equilibrium, which allowed for structural analysis of both states independently. Our new insights in tetramer conformations provided understanding of its DNA-binding kinetics. Using the stable MutS dimer, we analyzed kinetics of binding to different mismatches and ATP-dependent sliding clamp formation as summarized in Figure 7.

We used solution scattering and crystallography to obtain structural information on the full-length dimeric MutS protein. Combined, these techniques are powerful tools to provide complete models for shape and conformation of proteins as has been described in several reviews (52,53). The SAXS data indicated that in solution, the C-termini of full-length MutS occupy space in line with the DNA-clamp domains, thus extending the dimer. The crystal structure of full-length MutS showed an alternate position of the C-terminal domains stabilized by crystal contacts, indicating that there is mobility of the C-terminal domains with respect to the rest of the dimer. Nonetheless, the use of stable full-length dimer mutants opens possibilities to address structural questions that cannot be answered when working with the C-terminally truncated MutS dimer. One such question regards the interaction with the β-clamp, which has been reported to involve residues within the C-terminus (54) and has recently been shown to be important for the efficiency of MMR *in vivo* (55).

SAXS analysis of the stable cross-linked tetramer indicated a predominantly extended shape, with the two dimers facing away from each other. This confirms SAXS assays by Mendillo *et al.* (8), who used the C-terminal domain alone, as fusion proteins or wild-type MutS where the tetramers were mixed with dimeric MutS. We observed that when bound to 21-bp DNA, more features

could be observed in the SAXS curve, probably caused by stabilization of the DNA-binding clamp domains. The resulting distance distribution plot of our measurement with the tetramer-21-bp DNA complex is in good agreement with the predicted distance distribution plot for an extended arrangement based on the crystal structure of MutS bound to DNA (8).

Although no single model adequately describes the tetramer bound to 60-bp DNA, the SAXS data indicate an increase in the maximum dimension to almost twice the length of a single tetramer. This suggests that the tetramer remains mostly extended when bound to DNA, as bending over to bind the DNA in both sites would instead have reduced the maximum dimension of the complex. This is in agreement with AFM studies, in which tetramers of wild-type MutS showed one of its dimers contacting the DNA while overall shape appeared to be extended (45). Nevertheless, detailed ensemble optimization method analysis of our SAXS data suggests the presence of smaller population of free tetrameric MutS in a bent-over conformation. As cross-links could be made between residues 162 within tetramers, it is likely that the MutS tetramer occasionally bends over.

In our SPR experiments, bending over of the two dimers within the MutS tetramer and the subsequent possibility for bivalent binding of the DNA can explain its slow dissociation from DNA (as illustrated in Figure 7B). Although such bending over is only a rare event in solution, as shown in the SAXS analysis, in the SPR experiments we enrich for the bent-over tetramers, as this two-site DNA-bound species binds stronger. The extra parameters in the kinetic model for tetramer binding made the fit possible, but we are hesitant to interpret the exact meaning of the rate constants of the steps involved, as they can be further modulated by other factors that may play a role, such as bending of DNA (44). Nevertheless, our more detailed analysis of the tetramer shape begins to explain the unexpected kinetics of this form on DNA.

Such complex kinetics was not observed for a single DNA-binding unit of MutS, the dimer. Therefore, the dimeric MutS mutants are of great value to investigate factors that influence efficiency in recognition or sliding clamp formation. As has been reported before (20), we find that MutS recognizes specific mismatches better than others with differences in K_d^{app}. The fact that affinities diverge is interesting, as the binding mode of MutS is similar for all mismatches (6). It could mean that some mismatches adapt to the protein-bound state more efficiently than others. The correlation between slow dissociation rates and strong affinities suggests that differences in dissociation rates contribute to the differential mismatch affinities, which is in agreement with what has been found by Huang and Crothers (20) and what has been reported for human MutS homologs (48).

In our experiments, the flanking sequences of the mismatch influenced recognition by the MutS dimer, as had been indicated previously for wild-type MutS (47,50) and has also been described for MutSα (48). As we saw that the influence of flanking sequences is larger on some mismatches than for others, as is the influence of ATP, comparisons between affinities for mismatches should always be made with care.

In the presence of ATP, mismatch-bound MutS can undergo a conformational change to form a sliding clamp on DNA (7,51). The dissociation rates of the sliding clamps from end-blocked DNA is 10 times faster in our experiments than what has been reported previously (7,42,56). This is probably due to partial dissociation of the sliding clamps at the ssDNA linkers in our SPR setup (7), but such dissociation would be consistent for all mismatches. We saw that at low ATP concentrations, the efficiency of clamp formation can differ, but at concentrations above 12.8 μM ATP concentration, almost all of the MutS protein released as sliding clamps from the mismatches that we tested in this manner. This means that at cellular ATP concentrations [0.5–3 mM in *E. coli* (57)], sliding-clamp formation is not a limiting factor to initiate subsequent steps.

As for the CC mismatch, ATP-independent release was already faster than $0.4\,s^{-1}$, the same ATP-dependent dissociation experiment could not be performed. However, in the experiments with excess ATP and end-blocked DNA, only for this mismatch no stable sliding clamp formation was observed (as illustrated in Figure 7A). This may explain the inefficient repair of the CC mismatch (46). This lack of sliding clamp formation can not be explained solely by the low affinity of MutS for this mismatch, as a similar low affinity was measured in presence of ATP for binding a TT mismatch for which clamp formation was not impaired. It has, however, been reported that MutS still kinks DNA when binding a CC mismatch (20), indicating that MutS does bind CC differently than homoduplex. MutS in solution shows fast ATP hydrolysis but slow nucleotide exchange (40); therefore, in our experiment, MutS does not contain ATP in initial binding. After mismatch recognition, MutS readily binds ATP followed by the conformational change to a sliding clamp. As the recognition steps are not abnormal for the C·C mismatch, it may be that either subsequent ATP binding or the conformational change is not efficient.

Concluding, we have investigated both the full-length dimer of MutS and the tetramer of MutS separately. The bacterial mismatch repair system is easy to modify and isolate for *in vitro* assays, allowing for ways to uncouple functions of MutS. Using the stable dimer, we find that it is not mismatch binding, but the ability to undergo the correct conformational change on ATP binding that is correlated to mismatch repair efficiency. Again this indicates the importance of proper mismatch verification and signaling (41,58) to achieve specificity during this complicated DNA repair process.

ACCESSION NUMBERS

The coordinates of the crystal structure of MutS D835R have been deposited in the PDB with entry code 3ZLJ.

SUPPLEMENTARY DATA

Supplementary Data are available at NAR Online, including [60–62].

ACKNOWLEDGEMENTS

The authors thank Prakash Rucktooa and Robbie Joosten for assistance with crystallographic data processing and structure refinement, members of the Sixma and Perrakis laboratories for discussions on the project and Anastassis Perrakis for critical reading of the manuscript. They thank the beamline scientists from ID14-4 at ESRF for technical support during data collection.

FUNDING

European Community's Seventh Framework Programme MM2M [HEALTH-F4-2008-223545] and BioStruct-X [FP7-INFRASTRUCTURES-2011-1-283570]; The Netherlands Organisation for Scientific Research - Chemical Sciences [711.011.011 and 700.58.428]; and funding of the Centre for Biomedical Genetics. Funding for open access charge: Institute funding.

Conflict of interest statement. None declared.

REFERENCES

1. Kunkel,T.A. and Erie,D.A. (2005) DNA mismatch repair. *Annu. Rev. Phys. Chem.*, **74**, 681–710.
2. Lynch,H.T. and la Chapelle,de,A. (1999) Genetic susceptibility to non-polyposis colorectal cancer. *J. Med. Genet.*, **36**, 801–818.
3. Jiricny,J. (2006) The multifaceted mismatch-repair system. *Nat. Rev. Mol. Cell. Biol.*, **7**, 335–346.
4. Lamers,M.H., Perrakis,A., Enzlin,J.H., Winterwerp,H.H.K., de Wind,N. and Sixma,T.K. (2000) The crystal structure of DNA mismatch repair protein MutS binding to a G·T mismatch. *Nature*, **407**, 711–717.
5. Obmolova,G., Ban,C., Hsieh,P. and Yang,W. (2000) Crystal structures of mismatch repair protein MutS and its complex with a substrate DNA. *Nature*, **407**, 703–710.
6. Natrajan,G., Lamers,M.H., Enzlin,J.H., Winterwerp,H.H.K., Perrakis,A. and Sixma,T.K. (2003) Structures of *Escherichia coli* DNA mismatch repair enzyme MutS in complex with different mismatches: a common recognition mode for diverse substrates. *Nucleic Acids Res.*, **31**, 4814–4821.
7. Jeong,C., Cho,W., Song,K., Cook,C., Yoon,T., Ban,C., Fishel,R. and Lee,J. (2011) MutS switches between two fundamentally distinct clamps during mismatch repair. *Nat. Struct. Mol. Biol.*, **18**, 379–385.
8. Mendillo,M.L., Putnam,C.D. and Kolodner,R.D. (2007) *Escherichia coli* MutS tetramerization domain structure reveals that stable dimers but not tetramers are essential for DNA mismatch repair *in vivo*. *J. Biol. Chem.*, **282**, 16345–16354.
9. Calmann,M.A., Nowosielska,A. and Marinus,M.G. (2005) The MutS C terminus is essential for mismatch repair activity in vivo. *J. Bacteriol.*, **187**, 6577–6579.
10. Bjornson,K.P., Blackwell,L.J., Sage,H., Baitinger,C., Allen,D. and Modrich,P. (2003) Assembly and molecular activities of the MutS tetramer. *J. Biol. Chem.*, **278**, 34667–34673.
11. Biswas,I., Ban,C., Fleming,K.G., Qin,J., Lary,J.W., Yphantis,D.A., Yang,W. and Hsieh,P. (1999) Oligomerization of a MutS mismatch repair protein from *Thermus aquaticus*. *J. Biol. Chem.*, **274**, 23673–23678.
12. Takamatsu,S., Kato,R. and Kuramitsu,S. (1996) Mismatch DNA recognition protein from an extremely thermophilic bacterium, *Thermus thermophilus* HB8. *Nucleic Acids Res.*, **24**, 640–647.
13. Miguel,V., Monti,M.R. and Argaraña,C.E. (2008) The role of MutS oligomers on *Pseudomonas aeruginosa* mismatch repair System activity. *DNA Repair*, **7**, 1799–1808.
14. Feng,G., Tiffany Tsui,H. and Winkler,M.E. (1996) Depletion of the cellular amounts of the MutS and MutH methyl-directed mismatch repair proteins in stationary-phase *Escherichia coli* K-12 cells. *J. Bacteriol.*, **178**, 2388–2396.
15. Jiang,Y. and Marszalek,P.E. (2011) Atomic force microscopy captures MutS tetramers initiating DNA mismatch repair. *EMBO J.*, **30**, 2881–2893.
16. Calmann,M.A., Nowosielska,A. and Marinus,M.G. (2005) Separation of mutation avoidance and antirecombination functions in an *Escherichia coli mutS* mutant. *Nucleic Acids Res.*, **33**, 1193–1200.
17. Manelyte,L., Urbanke,C., Giron-Monzon,L. and Friedhoff,P. (2006) Structural and functional analysis of the MutS C-terminal tetramerization domain. *Nucleic Acids Res.*, **34**, 5270–5279.
18. Miguel,V., Pezza,R.J. and Argaraña,C.E. (2007) The C-terminal region of *Escherichia coli* MutS and protein oligomerization. *Biochem. Biophys. Res. Commun.*, **360**, 412–417.
19. Gupta,S., Gellert,M. and Yang,W. (2011) Mechanism of mismatch recognition revealed by human MutSβ bound to unpaired DNA loops. *Nat. Struct. Mol. Biol.*, **19**, 72–78.
20. Huang,S.N. and Crothers,D.M. (2008) The role of nucleotide cofactor binding in cooperativity and specificity of MutS recognition. *J. Mol. Biol.*, **384**, 31–47.
21. Winkler,I., Marx,A.D., Lariviere,D., Heinze,R., Cristovao,M., Reumer,A., Curth,U., Sixma,T.K. and Friedhoff,P. (2011) Chemical trapping of the dynamic MutS-MutL complex formed in DNA mismatch repair in *Escherichia coli*. *J. Biol. Chem.*, **286**, 17326–17337.
22. Kabsch,W. (2010) XDS. *Acta Crystallogr. Sect. D Biol. Crystallogr.*, **66**, 125–132.
23. Evans,P. (2005) Scaling and assessment of data quality. *Acta Crystallogr. Sect. D Biol. Crystallogr.*, **62**, 72–82.
24. CCP4. (1994) Coot: model-building tools for molecular graphics. *Acta Crystallogr. Sect. D Biol. Crystallogr.*, **50**, 760–763.
25. McCoy,A.J., Grosse-Kunstleve,R.W., Adams,P.D., Winn,M.D., Storoni,L.C. and Read,R.J. (2007) Phaser crystallographic software. *J. Appl. Crystallogr.*, **40**, 658–674.
26. Murshudov,G.N., Vagin,A.A. and Dodson,E.J. (1997) Refinement of macromolecular structures by the maximum-likelihood method. *Acta Crystallogr. Sect. D Biol. Crystallogr.*, **53**, 240–255.
27. Joosten,R.P., Salzemann,J., Bloch,V., Stockinger,H., Berglund,A.C., Blanchet,C., Bongcam-Rudloff,E., Combet,C., Da Costa,A.L., Deleage,G. *et al.* (2009) PDB_REDO: automated re-refinement of X-ray structure models in the PDB. *J. Appl. Crystallogr.*, **42**, 376–384.
28. Emsley,P. and Cowtan,K. (2004) Coot: model-building tools for molecular graphics. *Acta Crystallogr. Sect. D Biol. Crystallogr.*, **60**, 2126–2132.
29. Chen,V.B., Arendall,W.B., Headd,J.J., Keedy,D.A., Immormino,R.M., Kapral,G.J., Murray,L.W., Richardson,J.S. and Richardson,D.C. (2009) MolProbity: all-atom structure validation for macromolecular crystallography. *Acta Crystallogr. Sect. D Biol. Crystallogr.*, **66**, 12–21.
30. Blanchet,C.E., Zozulya,A.V., Kikhney,A.G., Franke,D., Konarev,P.V., Shang,W.F., Klaering,R., Robrahn,B., Hermes,C., Cipriani,F. *et al.* (2012) Instrumental setup for high-throughput small- and wide-angle solution scattering at the X33 beamline of EMBL Hamburg. *J. appl. Crystallogr.*, **45**, 489–495.
31. Petoukhov,M.V., Franke,D., Shkumatov,A.V., Tria,G., Kikhney,A.G., Gajda,M., Gorba,C., Mertens,H.D.T., Konarev,P.V. and Svergun,D.I. (2012) New developments in the *ATSAS* program package for small-angle scattering data analysis. *J. Appl. Crystallogr.*, **45**, 342–350.
32. Konarev,P.V., Volkov,V.V., Sokolova,A.V., Koch,M.H.J. and Svergun,D.I. (2003) *PRIMUS*: a Windows PC-based system for small-angle scattering data analysis. *J. appl. Crystallogr.*, **36**, 1277–1282.
33. Svergun,D.I. (1992) Determination of the regularization parameter in indirect-transform methods using perceptual criteria. *J. Appl. Crystallogr.*, **25**, 495–503.

34. Franke,D. and Svergun,D.I. (2009) *DAMMIF*, a program for rapid *ab-initio* shape determination in small-angle scattering. *J. Appl. Crystallogr.*, **42**, 342–346.
35. Volkov,V.V. and Svergun,D.I. (2003) Uniqueness of *ab initio* shape determination in small-angle scattering. *J. Appl. Crystallogr.*, **36**, 860–864.
36. Motulsky,H. (1999) *Analyzing data with GraphPad prism*. GraphPad Software Inc.
37. Svitel,J., Andrea Balbo,A., Mariuzza,R.A., Gonzales,N.R. and Schuck,P. (2003) Combined affinity and rate constant distributions of ligand populations from experimental surface binding kinetics and equilibria. *Biophys. J.*, **84**, 4062–4077.
38. Svitel,J., Boukari,H., Van Ryk,D., Willson,R.C. and Schuck,P. (2007) Probing the functional heterogeneity of surface binding sites by analysis of experimental binding traces and the effect of mass transport limitation. *Biophys. J.*, **92**, 1742–1758.
39. Lamers,M.H., Georgijevic,D., Lebbink,J.H., Winterwerp,H.H.K., Agianian,B., de Wind,N. and Sixma,T.K. (2004) ATP increases the affinity between MutS ATPase domains: Implications for ATP hydrolysis and conformational changes. *J. Biol. Chem.*, **279**, 43879–438885.
40. Lamers,M.H., Winterwerp,H.H.K. and Sixma,T.K. (2003) The alternating ATPase domains of MutS control DNA mismatch repair. *EMBO J.*, **22**, 746–756.
41. Lebbink,J.H.G., Georgijevic,D., Natrajan,G., Fish,A., Winterwerp,H.H.K., Sixma,T.K. and de Wind,N. (2006) Dual role of MutS glutamate 38 in DNA mismatch discrimination and in the authorization of repair. *EMBO J.*, **25**, 409–419.
42. Lebbink,J.H.G., Fish,A., Reumer,A., Natrajan,G., Winterwerp,H.H. and Sixma,T.K. (2010) Magnesium coordination controls the molecular switch function of DNA mismatch repair protein MutS. *J. Biol. Chem.*, **285**, 13131–13141.
43. Monti,M.C., Cohen,S.X., Fish,A., Winterwerp,H.H.K., Barendregt,A., Friedhoff,P., Perrakis,A., Heck,A.J.R., Sixma,T.K., van den Heuvel,R.H.H. *et al.* (2011) Native mass spectrometry provides direct evidence for DNA mismatch-induced regulation of asymmetric nucleotide binding in mismatch repair protein MutS. *Nucleic Acids Res.*, **39**, 8052–8064.
44. Vafabakhsh,R. and Ha,T. (2012) Extreme bendability of DNA less than 100 base pairs Long revealed by single-molecule cyclization. *Science*, **337**, 1097–1101.
45. Wang,H., Yang,Y., Schofield,M.J., Du,C., Fridman,Y., Lee,S.D., Larson,E.D., Drummond,J.T., Alani,E., Hsieh,P. *et al.* (2003) DNA bending and unbending by MutS govern mismatch recognition and specificity. *Proc. Natl Acad. Sci. USA*, **100**, 14822–14827.
46. Su,S., Lahue,R.S., Au,K.G. and Modrich,P. (1987) Mispair specificity of methyl-directed DNA mismatch correction *in vitro*. *J. Biol. Chem.*, **263**, 6829–6835.
47. Joshi,A. and Rao,B.J. (2001) MutS recognition: multiple mismatches and sequence context effects. *J. Biosci.*, **26**, 595–606.
48. Mazurek,A., Johnson,C.N., Germann,M.W. and Fishel,R. (2009) Sequence context effect for hMSH2-hMSH6 mismatch-dependent activation. *Proc. Natl Acad. Sci. USA*, **106**, 4177–4182.
49. Cristovao,M., Sisamakis,E., Hingorani,M.M., Marx,A.D., Jung,C.P., Rothwell,P.J., Seidel,C.A.M. and Friedhoff,P. (2012) Single-molecule multiparameter fluorescence spectroscopy reveals directional MutS binding to mismatched bases in DNA. *Nucleic Acids Res.*, **40**, 5448–5464.
50. Brown,J., Brown,T. and Fox,K.R. (2001) Affinity of mismatch-binding protein MutS for heteroduplexes containing different mismatches. *Biochem. J.*, **354**, 627–633.
51. Biswas,I. and Vijayvargia,R. (2000) Heteroduplex DNA and ATP induced conformational changes of a MutS mismatch repair protein from *Thermus aquaticus*. *Biochem. J.*, **347**, 881–886.
52. Petoukhov,M.V. and Svergun,D.I. (2013) Applications of small-angle X-ray scattering to biomacromolecular solutions. *Int. J. Biochem. Cell Biol.*, **45**, 429–437.
53. Blanchet,C.E. and Svergun,D.I. (2013) Small-angle X-Ray scattering on biological macromolecules and nanocomposites in solution. *Annu. Rev. Phys. Chem.*, **64**, 37–54.
54. López de Saro,F.J., Marinus,M.G., Modrich,P. and O'Donnell,M. (2006) The β sliding clamp binds to multiple sites within MutL and MutS. *J. Biol. Chem.*, **281**, 14340–14349.
55. Lenhart,J.S., Sharma,A., Hingorani,M.M. and Simmons,L.A. (2012) DnaN clamp zones provide a platform for spatiotemporal coupling of mismatch detection to DNA replication. *Mol. Microbiol.*, **87**, 553–568.
56. Cho,W., Jeong,C., Kim,D., Chang,M., Song,K., Hanne,J., Ban,C., Fishel,R. and Lee,J. (2012) ATP alters the diffusion mechanics of MutS on mismatched DNA. *Structure*, **20**, 1–11.
57. Lasko,R.D. and Wang,D.I.C. (1996) On-line monitoring of intracelIuIar ATP concentration in *Escherichia coIi* fermentations. *Biotechnol. Bioeng.*, **52**, 364–372.
58. Junop,M.S., Obmolova,G., Rausch,K., Hsieh,P. and Yang,W. (2001) Composite active site of an ABC ATPase: MutS uses ATP to verify mismatch recognition and authorize DNA repair. *Mol. Cell*, **7**, 1–12.
59. Loh,T., Murphy,K.C. and Marinus,M.G. (2001) Mutational Analysis of the MutH Protein from *Escherichia coli*. *J. Biol. Chem.*, **276**, 12113–12119.
60. Feng,G. and Winkler,M.E. (1995) Single-step purifications of His6-MutH, His6-MutL and His6-MutS repair proteins of *Escherichia coli* K-12. *BioTechniques*, **6**, 956–965.
61. Xiao,Y., Jung,C., Marx,A.D., Winkler,I., Wyman,C., Lebbink,J.H.G., Friedhoff,P. and Cristovao,M. (2011) Generation of DNA nanocircles containing mismatched bases. *BioTechniques*, **51**, 259–265.